An orbital release model for the Orion BN/KL fingers

A. C. Raga, P. R. Rivera-Ortiz, J. Cantó, A. Rodríguez-González, A. Castellanos-Ramírez

Monthly Notices of the ROYAL ASTRONOMICAL SOCIETY

MNRAS **508,** L74–L78 (2021) https://doi.org/10.1093/mnrasl/slab072
Advance Access publication 2021 July 26

An orbital release model for the Orion BN/KL fingers

A. C. Raga,[1]★ P. R. Rivera-Ortiz,[2] J. Cantó,[3] A. Rodríguez-González[1] and A. Castellanos-Ramírez[3]

[1]*Instituto de Ciencias Nucleares, Universidad Nacional Autónoma de México, AP 70-543, CDMX 04510, México*
[2]*Observatoire de Grenoble, Grenoble Alpes, CNRS, IPAG, F-38000 Grenoble, France*
[3]*Instituto de Astronomía, Universidad Nacional Autónoma de México, AP 70-264, CDMX 04510, México*

Accepted 2021 June 19. Received 2021 June 19; in original form 2021 June 7

ABSTRACT

We present a simple model in which the bullets that produce the 'Orion fingers' (ejected by the BN/KL object) are interpreted as protoplanets or low-mass protostars in orbit around a high-mass star that has a supernova explosion. As the remnant of the SN explosion has only a small fraction of the mass of the pre-supernova star, the orbiting objects then move away in free trajectories, preserving their orbital velocity at the time of release. We show that a system of objects arranged in approximately coplanar orbits results in trajectories with morphological and kinematical characteristics resembling the Orion fingers. We show that, under the assumption of constant velocity motions, the positions of the observed heads of the fingers can be used to reconstruct the properties of the orbital structure from which they originated, resulting in a compact disc with an outer radius of ∼2.4 au.

Key words: stars: winds, outflows – ISM: individual objects: Orion BN/KL – ISM: jets and outflows.

1 INTRODUCTION

One of the more intriguing flows in the Galactic interstellar medium is composed of the 'fingers' radiating away from the Orion BN/KL object (a massive embedded stellar object surrounded by a compact nebula; see Becklin & Neugebauer 1967; Kleinmann & Low 1967). These fingers were first reported by Allen & Burton (1993) in infrared (IR) H_2 and [FeII] emission, and have lengths of up to ∼2 arcmin (∼7×10^{17} cm at a distance of 400 pc). The bases of these fingers, as well as a multitude of other filaments, are detected in interferometric carbon monoxide (CO) observations (Zapata et al. 2009, 2017; Bally et al. 2017). The CO emission of the individual fingers shows a remarkable 'Hubble law' of linearly increasing radial velocities with distance from the BN/KL object.

Doi et al. (2002) and Bally et al. (2011, 2015) obtained proper motions of the IR line emission of the heads of the 'Orion fingers', and Nissen et al. (2007) obtained radial velocities of these features. Nissen et al. (2012) combined proper motion and radial velocity measurements to obtain the full spatial motion of some of the fingers.

The fact that the motions of the heads of the individual fingers give similar dynamical time-scales implies that they were all ejected in an 'explosive' event of short duration. This result stands regardless of the fact that some of the 'bullets' at the tips of the fingers might have had a substantial slowing down along their trajectories (Rivera-Ortiz et al. 2019a,b).

It has been proposed that this sudden event could have been

(i) a result of the break-up of a multiple stellar system (see Reipurth et al. 2010; Moeckel & Goddi 2012; Reipurth & Mikkola 2012, 2015). The dynamics of a three- or four-body system can explain the high velocities of the stars near the BN/KL object (observed in radio continuum by Rodríguez et al. 2005 and by Gómez et al. 2005, 2008), and in principle could trigger the 'interstellar bullets' that create the Orion fingers. A first attempt to model the ejection of a cluster of bullets through a gravitational interaction was recently presented by Rivera-Ortiz et al. (2021);

(ii) a result of a supernova, which could liberate the bound orbital motion of companion stars into free hyperbolic orbits. This scenario can explain the high velocities of the stars around BN/KL, and could result in the ejection of the observed high-velocity bullets as well.

These scenarios are discussed in the previous literature on the Orion fingers (see e.g. Bally et al. 2011, 2017; Zapata et al. 2017).

A remarkable feature of the outflow from BN/KL is that while the whole system of fingers shows an elongated morphology towards the NW and SE, this roughly bipolar structure does not correspond to a division between blueshifted emission and redshifted emission. There is a 'red/blueshift' division in the system of fingers, but with respect to an axis roughly aligned with the NW/SE elongation. This NE/SW division of the blue (NE) and redshifted (SW) emission is clearly seen in fig. 3 of Zapata et al. (2017). However, there are some filaments with the 'wrong radial velocity shift' (i.e. some redshifted filaments to the NE and some blueshifted filaments to the SW), as can be seen in the observations of Bally et al. (2017).

In this paper, we show that the elongated morphology and 'side-to-side' red/blueshifted kinematics of the system of Orion fingers can be straightforwardly explained as the free propagation of a system of objects with a planar initial velocity distribution. In Section 2, we show how this extremely simple model produces spatial and radial velocity distributions that qualitatively resemble the system of Orion fingers. Section 3 derives the relation between the radial (position) distribution function and the orbital velocity distribution of a system of massless particles in circular orbits around a massive object. In Section 4, we show how under the assumption of a planar velocity distribution and free post-supernova trajectories the observed positions (and also velocity information if available) can

★ E-mail: raga@nucleares.unam.mx

be used to reconstruct the velocity distribution of the bullet system. In Section 5, we use the observed positions of the tips of the Orion fingers to reconstruct their velocity distribution and the radial position distribution of the bullets on the pre-release circumstellar disc. The results are discussed in Section 6.

2 INSTANTANEOUS RELEASE MODEL

2.1 General considerations

We assume that we have a system of N non-interacting particles with initial (at $t = 0$) positions $\underline{x}_{0,i}$ and velocities $\underline{v}_i$ (with $i = 1, \ldots N$). For $t > 0$, the free particles then have (vector) positions

$$\underline{x}_i(t) = \underline{x}_{0,i} + t\,\underline{v}_i\,. \tag{1}$$

If initially the particles lie within a volume of size L, it is clear that for $t \gg L/v_{\rm m}$ (where $v_{\rm m}$ is the smallest modulus of all of the particle velocities) the first term on the right-hand side of equation (1) can be neglected, and we have trajectories that are independent of the initial positions of the particles, and only depend on their initial velocities.

We present two examples of this trivial model, 'thin disc' (Section 2.2) and 'thick disc' initial distributions (Section 2.3). The thin disc distribution has a system of particles in coplanar circular orbits around a central star, and the thick disc distribution has circular orbits with a range of inclinations of their orbital axes. At $t = 0$, the central star has a supernova explosion, ejecting most of its mass: A remnant of only $\sim$2 $M_\odot$ will be left behind when an $\sim$30 $M_\odot$ solar metallicity star has an SN explosion (see e.g. Liu et al. 2021, and references therein). With such a drastic decrease in the mass of the central star, the orbiting particles will suddenly find themselves in free, very open hyperbolic orbits, which can be approximated as linear trajectories.

The question then is what are these particles in initial circular orbits around the pre-supernova, massive star: Obvious candidates are giant planets/protoplanets and/or very low mass stars forming in a disc around the massive star. This gives the attractive picture of the Orion fingers being produced by ejected pre-planetary or pre-stellar condensations.

2.2 Planar distribution with circular orbits

We now consider a planar distribution of 100 massless particles orbiting around a central star of mass M_*, with orbital radii r distributed randomly in the $0 \rightarrow R_0$ range. The phase of the orbit at $t = 0$ is chosen uniformly in the $0 \rightarrow 2\pi$ range. Their orbital velocities then are

$$v_{\rm orb} = v_0 \sqrt{\frac{R_0}{r}}\,, \tag{2}$$

with

$$v_0 \equiv \sqrt{\frac{G M_*}{R_0}}\,. \tag{3}$$

The combination of v_0 and R_0 gives a characteristic time

$$t_0 \equiv \frac{R_0}{v_0} = \sqrt{\frac{R_0^3}{G M_*}}\,. \tag{4}$$

For example, for a distribution of particles with an outer radius $R_0 = 100$ au orbiting around a central star with an $M_* = 30\,M_\odot$ mass, we have $v_0 = 16.3\,{\rm km\,s^{-1}}$ and $t_0 = 29.1$ yr.

Assuming that at $t = 0$ the central star suddenly 'disappears', the particles then evolve with straight trajectories, preserving their initial velocity. Fig. 1 shows the particle trajectories up to a time $300\,t_0$, projected on to the plane of the sky for four different assumed angles between the disc axis and the line of sight.

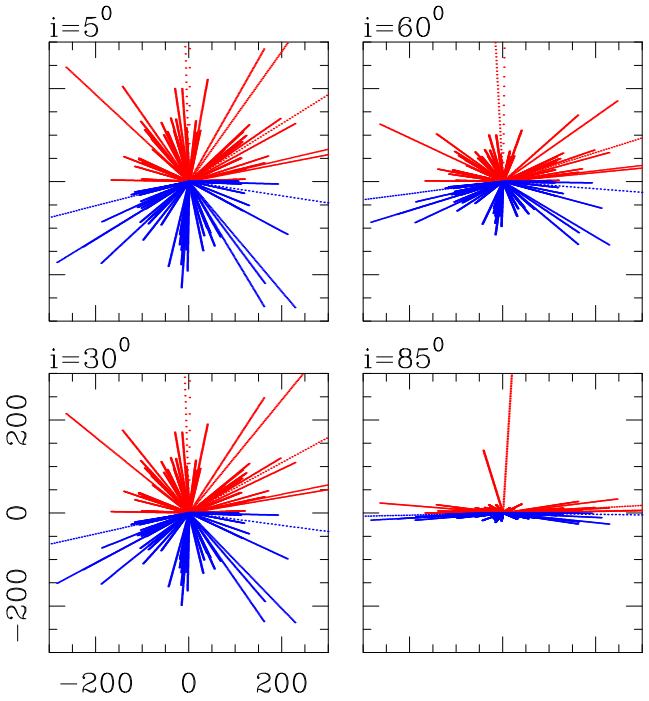

Figure 1. Trajectories of a system of free particles originating from a thin disc of outer radius R_0 and outer orbital velocity v_0 released at $t = 0$ and ending at $300\,t_0$ (see the text). The four frames show the projected trajectories for four different values of the inclination of the initial orbital axis with respect to the line of sight. The colours of the trajectories correspond to positive (red) and negative (blue) radial velocities of the ejected particles. The (x', y') plane of the sky axes is labelled in units of R_0.

2.3 Non-planar distribution with circular orbits

We now consider the same problem of 100 massless particles in initial circular orbits (which are 'liberated' at $t = 0$; see Section 2.2), but allowing the individual orbits to have axes with random tilts in the $0 \rightarrow 35^\circ$ range with respect to the average disc axis.

The resulting particle trajectories at $t = 300\,t_0$ (see equation 4) are shown in Fig. 2. We see that the variation in the initial orbital axes of the particles results in a partial mixing of redshifted and blueshifted particles above/below the $y' = 0$ axis. This effect is more strongly pronounced at the smaller and larger values of the inclination ($i = 5$ and 85°; see Fig. 2).

3 THE RELATION BETWEEN THE RADIAL DENSITY AND VELOCITY DISTRIBUTIONS OF PARTICLES IN AN ORBITAL DISC

In Section 2.2, we considered a set of N particles in coplanar circular orbits around a central source, with a uniform radial distribution. Let us now look at a more general problem, in which the radial particle distribution has an arbitrary power-law form:

$$f(r) = \frac{(\alpha + 1)N}{R_0^{\alpha+1}} r^\alpha, \tag{5}$$

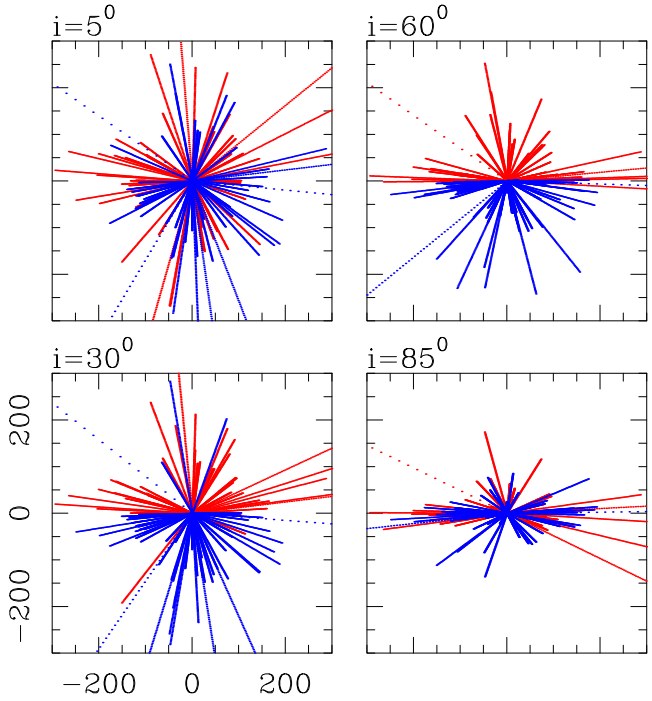

Figure 2. The same as Fig. 1 but for an initial 'thick disc' distribution of orbits with axes with random tilts of up to 35° with respect to the disc axis.

where the proportionality constant is determined from the $\int_0^{R_0} f(r)\mathrm{d}r = N$ condition, with r being the radius on the orbital plane and R_0 being the radius of the outer orbit of the N particles.

It is straightforward to show that this distribution corresponds to a surface number density of particles:

$$n(r) = \frac{(\alpha+1)N}{2\pi R_0^{\alpha+1}} r^{\alpha-1}. \tag{6}$$

As the particles are in circular orbits, their velocity as a function of r is given by equation (2). We can then calculate the distribution $g(v)$ of the modulus v of the velocities of the particles as

$$g(v) = \frac{f(v)}{|\mathrm{d}v/\mathrm{d}r|} = \frac{2(\alpha+1)N v_0^{2+2\alpha}}{v^{3+2\alpha}}, \tag{7}$$

where equations (2) and (5) have been used for the second equality. For the case of a uniform radial particle distribution (with $\alpha = 0$) described in Section 2.2, this gives

$$g(v) = \frac{2N v_0^2}{v^3}. \tag{8}$$

4 RECONSTRUCTING THE ORBITAL DISC FROM THE EVOLVED TRAJECTORIES

4.1 The ballistic trajectories

We now consider the ballistic trajectories of particles at large times, when they have reached distances $L \gg R_0$, where R_0 is the size of the original disc around a star that at $t = 0$ became an SN, thus releasing the particles from the central, stellar potential. For $t \gg t_0$ (see equations 1 and 4), the trajectory of a particle is

$$x(t) = tv\cos\theta\,; \quad y(t) = tv\sin\theta\,, \tag{9}$$

where θ is the (random) angle between the orbital velocity and the x-axis and v is the modulus of the orbital velocity of one of the particles.

If we assume that the initial disc is at an inclination i with respect to the line of sight (with the y-axis into and the x-axis on the plane of the sky), the plane of the sky trajectory will be

$$x'(t) = x(t)\,; \quad y'(t) = y(t)\cos i. \tag{10}$$

The parcel has plane of the sky velocities

$$v_{x'} = v\cos\theta\,; \quad v_{y'} = v\sin\theta\cos i, \tag{11}$$

a radial velocity (with positive values away from the observer)

$$v_\mathrm{r} = v\sin\theta\sin i\,, \tag{12}$$

and a proper motion velocity

$$v_\mathrm{pm} = v\sqrt{\cos^2\theta + \sin^2\theta\cos^2 i}\,. \tag{13}$$

Finally, from equation (11) we compute the average value over all bullets of the moduli of x' and y':

$$\begin{aligned} &< |x'| > = t < v >< |\cos\theta| >\,; \\ &< |y'| > = t < v >< |\sin\theta| > \cos i\,, \end{aligned} \tag{14}$$

where we have assumed that v and θ are uncorrelated. Also, $< |\cos\theta| > = < |\sin\theta| > = 2/\pi$ for random directions on a plane.

4.2 The reconstruction

We assume that at a time $t \gg t_0$ we observe the positions of a system of particles arising from an orbital disc system that at $t = 0$ lost its central gravitational binding source. We assume that we have the plane of the sky positions for N observed 'bullets'. If for these bullets we have observed proper motions and radial velocities, we can directly calculate the distribution function of the velocity moduli of the ensemble of particles.

If we have the radial velocities v_r and/or the proper motions v_pm for only some of the bullets (the proper motion of at least one bullet being necessary), using the assumption that the motions lie on a plane (i.e. the plane of an initial orbiting disc structure), we can still reconstruct the velocity distribution function. To this effect, we proceed with the following steps:

(i) Step 1: If the observed system lends itself to an interpretation as an 'unbound debris disc', we should observe a clear side-to-side division between positive and negative radial velocities (see Fig. 1). The line on which the radial velocities change sign defines the $\theta = 0$ direction, and then the (x', y') coordinates correspond to the distances along and across this axis (respectively), with the origin located at the point of divergence of the particle trajectories.

(ii) Step 2: We then use the bullets for which we have observed proper motions to calculate the time t since the gravitational release through the relation $t = \sqrt{x'^2 + y'^2}/v_\mathrm{pm}$, which (apart from being evidently correct) is obtained from equations (9), (10), and (13). For an instantaneous release model to be appropriate, similar values of t should be obtained for all of the bullets with observed proper motions.

(iii) Step 3: We now calculate the averages of the moduli of the plane of the sky (x', y') coordinates over all bullets (which we call $< |x'| >$ and $< |y'|$, respectively) and use equation (14) to find the inclination angle as

$$i = \cos^{-1}\left(\frac{< |y'| >}{< |x'| >}\right). \tag{15}$$

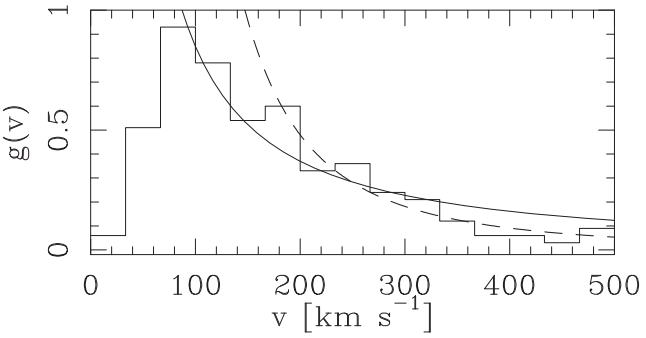

Figure 3. The histogram shows the velocity distribution function deduced from the observed positions of the tips of the Orion fingers. The solid and dashed curves show the power-law fits to the observed distribution function in the $v \geq 80$ and $v \geq 180\,\mathrm{km\,s^{-1}}$ velocity ranges (respectively).

(iv) Step 4: With the computed values of t and i, we now use the relation

$$v = \frac{|x'|}{t}\sqrt{1 + \frac{y'^2}{x'^2 \cos^2 i}}\,, \tag{16}$$

to calculate the full velocity v for all of the individual observed bullets (equation 16 can be directly obtained from equations 9 and 10). These velocities can be appropriately binned to obtain the empirical distribution function $g_e(v)$ of the velocities of the particles.

5 RECONSTRUCTION OF THE VELOCITY DISTRIBUTION OF THE ORION FINGERS

We took the data set of Bally et al. (2011; see their fig. 1), who analyse two epochs of H_2 images to obtain the positions and proper motions of the Orion finger bullets. We then followed the procedure described in Section 4:

(i) Step 1: From the CO radial velocities of Zapata et al. (2009, their fig. 1), we see that the change of sign in the radial velocities lies at a 52° angle (measured W from N). We then calculate the (x', y') coordinates of $N = 168$ bullets (with x' along the change of sign axis).

(ii) Step 2: We can obtain t from the positions and proper motion velocities of the bullets with equation (15). Most of the resulting ages are below 1000 yr, and we assumed a representative age of 500 yr, equal to the dynamical age of the protostellar objects around Orion BN/KL (see Rodríguez et al. 2005).

(iii) Step 3: We calculate the average values $< |x'| >$ and $< |y'| >$ of the moduli of the coordinates, and use equation (15) to obtain $i = 71°$.

(iv) Step 4: We calculate the moduli of the velocities of all particles with equation (16), and group them in 33 $\mathrm{km\,s^{-1}}$-wide bins to obtain the empirical velocity distribution function $g_e(v)$ (normalized so that $\int g_e(v) = N$, where $N = 168$ is the number of bullets in our sample). The resulting velocity distribution function is shown in Fig. 3.

The velocity distribution has a steep rise with increasing velocities, peaks at $v \approx 80\,\mathrm{km\,s^{-1}}$, and then has an approximately monotonic decrease for larger v (see Fig. 3). The initial rise in $g_e(v)$ probably corresponds to incompleteness in the data set, as a multitude of short, low-radial velocity filaments are present in the CO data (see e.g. Bally et al. 2017), and are not seen in H_2 images.

Because of this, we carry out power-law fits of the form

$$g(v) = B\left(\frac{200\,\mathrm{km\,s^{-1}}}{v}\right)^{\beta}\,, \tag{17}$$

to the empirical $g_e(v)$ setting a lower velocity cut-off $v_{\min}$ for the fit. We have tried following two values for this cut-off:

(i) ${v_{\min}}^{-1} = 80\,\mathrm{km\,s^{-1}}$, corresponding to the peak of the empirical $g_e(v)$,

(ii) ${v_{\min}}^{-2} = 180\,\mathrm{km\,s^{-1}}$, where the decrease of $g_e(v)$ shows an inflection.

As we can see in Fig. 3, the first fit clearly does not reproduce the decrease of the observed distribution $g_e(v)$ at velocities $>300\,\mathrm{km\,s^{-1}}$. For this reason, we favour the second fit, which does not reproduce the low velocity behaviour of $g_e(v)$, but this can be understood as being a result of an incompleteness in the sample of the shorter, lower velocity filaments and/or of a physical 'soft cut-off' of the distribution at lower velocities.

With this second fit (see the dashed line of Fig. 3), we obtain $B = 0.48 \pm 0.03\,\mathrm{km^{-1}\,s}$ and $\beta = 2.36 \pm 0.22$ (see equation 17). Using equations (7) and (17), we see that the exponent of the corresponding initial radial distribution of the bullets (see equation 5) is $\alpha = (\beta - 3)/2 = -0.32 \pm 0.02$. Also, comparing equations (7) and (17), from our fit we obtain a velocity (v_0) of $106 \pm 13\,\mathrm{km\,s^{-1}}$ at the outer edge of the initial disc. We should note that for calculating this velocity we used the $N = 168$ number of bullets in our sample, which probably has a substantial incompleteness. If we assume that the disc had a pre-supernova central star of $30\,M_\odot$, this outer edge velocity implies a disc radius of ∼2.4 au.

6 CONCLUSIONS

In a recent paper, Dempsey et al. (2020) modelled the propagation of orbital debris (protoplanets and/or planets) dispersed during the break-up of a multiple stellar system. We study a similar scenario, in which the planets or protoplanets orbit an embedded massive, pre-supernova star, and travel in approximately straight trajectories (preserving the modulus of their orbital velocity) when the supernova ejects most of the stellar mass. This scenario has no problem in reproducing the high velocities (of up to $\sim 500\,\mathrm{km\,s^{-1}}$) observed in the Orion fingers.

We argue that

(i) the elongated morphology and the division across the elongation axis into redshifted and blueshifted regions of the ensemble of fingers can be trivially explained as the free expansion of an approximately planar, orbital disc structure;

(ii) the velocity distribution of the heads of the Orion fingers implies a minimum orbital velocity of $\sim 100\,\mathrm{km\,s^{-1}}$, and therefore a maximum radius of ∼2.4 au (for an assumed $30\,M_\odot$ mass for the pre-supernova star).

From the observed velocity distribution, we find that the initial radial distribution of objects is approximately $\propto r^{\alpha}$, with $\alpha \sim -0.3$. This corresponds to a surface density of objects with a power-law exponent of ~ -1.3.

An interesting point is that there is currently no evidence of the existence of exoplanets or protoplanets orbiting massive stars or protostars. Possibly, the Orion fingers are evidence in favour of their existence. They imply the presence of ∼100–200 condensations within a few au from the star! A larger size for the initial disc structure is of course possible if a substantial outwards acceleration

of the condensations (i.e. the protoplanets) occurs when they interact with the expanding supernova ejection.

We should finally mention that two other systems of 'radiating fingers' have been detected in our Galaxy: DR 21 (Zapata et al. 2013; with only a few bullets) and G5.89 (Zapata et al. 2020; a system comparable to the Orion fingers). Based on these three detections, Zapata et al. (2020) conclude that these 'multifingered explosive events' have a frequency that is similar to the supernova rate of our Galaxy. This result also indicates that our model deserves further study.

ACKNOWLEDGEMENTS

AR and ARG acknowledge support from the PAPIIT (UNAM) project IA103121. PRO acknowledges funding from the European Research Council (ERC) under the European Union's Horizon 2020 research and innovation programme, for the Project 'The Dawn of Organic Chemistry' (DOC), grant agreement number 741002. ACR acknowledges support from a DGAPA, UNAM post-doctoral fellowship.

DATA AVAILABILITY

No new data were generated or analysed in support of this research.

REFERENCES

Allen D. A., Burton M. G., 1993, Nature, 363, 54
Bally J., Cunningham N. J., Moeckel N., Burton M. G., Smith N., Frank A., Nordlund A., 2011, ApJ, 727, 113
Bally J., Ginsburg A., Silvia D., Youngblood A., 2015, A&A, 579, A130
Bally J., Ginsburg A., Arce H., Eisner J., Youngblood A., Zapata L., Zinnecker H., 2017, ApJ, 837, 60
Becklin E. E., Neugebauer G., 1967, ApJ, 147, 799
Dempsey R., Zakamska N. L., Owen J. E., 2020, MNRAS, 495, 1172
Doi M., O'Dell C. R., Hartigan P., 2002, AJ, 124, 445
Gómez L., Rodríguez L. F., Loinard L., Lizano S., Poveda A., Allen C., 2005, ApJ, 635, 1166
Gómez L., Rodríguez L. F., Loinard L., Lizano S., Allen C., Poveda A., Menten K. M., 2008, ApJ, 685, 333
Kleinmann D. E., Low F., 1967, ApJ, 149, L1
Liu T., Wei Y.-F., Xue L., Sun M.-Y., 2021, ApJ, 908, 106
Nissen H. D., Gustafsson M., Lemaire J. L., Clénet Y., Rouan D., Field D., 2007, A&A, 466, 949
Nissen H. D., Cunningham N. J., Gustafsson M., Bally J., Lemaire J.-L., Favre C., Field D., 2012, A&A, 540, A119
Reipurth B., Mikkola S., 2012, Nature, 492, 221
Reipurth B., Mikkola S., 2015, AJ, 149, 145
Reipurth B., Mikkola S., Connelley M., Valtonen M., 2010, ApJ, 725, L56
Rivera-Ortiz P. R., Rodríguez-González A., Hernández-Martínez L., Cantó J., 2019a, ApJ, 874, 38
Rivera-Ortiz P. R., Rodríguez-González A., Hernández-Martínez L., Cantó J., Zapata L. A., 2019b, ApJ, 885, 104
Rivera-Ortiz P. R., Rodríguez-González A., Cantó J., Zapata L. A., 2021, ApJ, 916, 56
Rodríguez L. F., Poveda A., Lizano S., Allen C., 2005, ApJ, 627, L65
Zapata L. A., Schmid-Burgk J., Ho P. T. P., Rodríguez L. F., Menten K. M., 2009, ApJ, 704, L45
Zapata L. A., Schmid-Burgk J., Pérez-Goytia N., Ho P. T. P., Rodríguez L. F., Loinard L., Cruz-González I., 2013, ApJ, 765, L29
Zapata L. A., Schmid-Burgk J., Rodríguez L. F., Palau A., Loinard L., 2017, ApJ, 836, 133
Zapata L. A. et al., 2020, ApJ, 902, L47

This paper has been typeset from a TEX/LATEX file prepared by the author.